Journal of Materials Chemistry B

Accepted Manuscript

ROYAL SOCIETY OF CHEMISTRY

www.rsc.org/materialsB

Environmental Manipulation to Promote Stem Cell Survival *In Vivo*: Use of Aggregation, Oxygen Carrier, and BMP-2 Co-Delivery Strategies.

Ashley B. Allen, Ph.D.[1], Josh A. Zimmermann, M.S.[1,2], Olivia A. Burnsed, B.S.[1], Doron Cohn Yakubovich, B.S.[3], Hazel Y. Stevens, B.S.[4], Zulma Gazit, Ph.D.[3,5], Todd C. McDevitt, Ph.D.[1,2], Robert E. Guldberg, Ph.D.[4]

[1]Wallace H. Coulter Department of Biomedical Engineering, Parker H. Petit Institute for Bioengineering & Bioscience, Georgia Institute of Technology, Atlanta, GA, USA

[2]Gladstone Institute for Cardiovascular Disease, San Francisco, CA, USA

[3]Skeletal Biotech Laboratory, The Hebrew University-Hadassah Faculty of Dental Medicine, Jerusalem, Israel

[4]George W. Woodruff School of Mechanical Engineering, Parker H. Petit Institute for Bioengineering & Bioscience, Georgia Institute of Technology, Atlanta, GA, USA

[5]Regenerative Medicine Institute, Department of Surgery, Cedars-Sinai Medical Center, Los Angeles, CA, USA

Ashley B. Allen, Ph.D. Parker H. Petit Institute for Bioengineering & Bioscience, Georgia Institute of Technology, 315 Ferst Drive NW, Atlanta, GA 30332. Tel. 310-920-5962. Fax. 404-385-1397. aallen37@gatech.edu

Joshua A. Zimmermann, M.S. Gladstone Institute for Cardiovascular Disease, 1650 Owens Street, San Francisco, CA, 94158. Tel. 412-841-6778. josh.zimmermann@gladstone.ucsf.edu

Olivia A. Burnsed, B.S. Parker H. Petit Institute for Bioengineering & Bioscience, Georgia Institute of Technology, 315 Ferst Drive NW, Atlanta, GA 30332. Tel. 912-531-7647. Fax. 404-385-1397. olivia.burnsed@gatech.edu

Doron Cohn Yakubovich, B.S. Hadassah Medical Center, Hebrew University of Jerusalem, PO Box 12272, Ein Kerem, Jerusalem, 91120, Israel. Tel. +972-52-5986086. Fax. +972-52-6757628. doron.cohnyakubo@mail.huji.ac.il

Hazel Y. Stevens, B.S. Parker H. Petit Institute for Bioengineering & Bioscience, Georgia Institute of Technology, 315 Ferst Drive NW, Atlanta, GA 30332. Tel. 404-385-1327. Fax. 404-385-1397. hazel.stevens@me.gatech.edu

Zulma Gazit, Ph.D. Cedars-Sinai Medical Center, Regenerative Medicine Institute, 8700 Beverly Blvd. AHSP-8108, Los Angeles, CA 90048. Tel. 310-248-8576, Fax: (310) 248-8572. zulma.gazit@csmc.edu

Todd C. McDevitt, Ph.D. Gladstone Institute for Cardiovascular Disease, 1650 Owens Street, San Francisco, CA, 94158. Tel. 415-734-2875. todd.mcdevitt@gladstone.ucsf.edu

Robert E. Guldberg, Ph.D. Parker H. Petit Institute for Bioengineering & Bioscience, Georgia Institute of Technology, 315 Ferst Drive NW, Atlanta, GA 30332. Tel. 404-894-6589. Fax. 404-894-2291. robert.guldberg@me.gatech.edu

*Correspondence should be addressed to Robert E. Guldberg, Ph.D. Parker H. Petit Institute for Bioengineering & Bioscience, Georgia Institute of Technology, 315 Ferst Drive NW, Atlanta, GA 30332. Tel. 404-894-6589. Fax. 404-894-2291. robert.guldberg@me.gatech.edu

Abstract

While mesenchymal stem cell (MSC)-based strategies for critically-sized bone defect repair hold promise, poor cell survival *in vivo* remains a significant barrier to the translation of these therapeutics. One method employed to extend the survival of MSCs is the formation of three-dimensional aggregates, a strategy which modulates the immunomodulatory secretome of the cells, thereby influencing the local inflammatory environment and potentially bone tissue repair. Enrichment of cell-seeded hydrogels with oxygen carriers to counter the hypoxic conditions encountered *in vivo* or co-delivery of cells with growth factors, are also strategies employed to modulate the cell micro-environment. In this study, we examined the effect of human MSC (hMSC) and rat MSC (rMSC) aggregation on cell survival and bone tissue regeneration within both immunocompromised (nude) and syngeneic (Lewis) rat models. Despite a heightened release of paracrine factors from stem cell aggregates *in vitro*, the delivery of hMSC or rMSC aggregates in their respective rat models had no beneficial impact on cell survival, construct vascularization, or critically-sized bone defect repair. Co-delivery of oxygen carrier perfluorotributylamine (PFTBA) within the alginate hydrogel delivery vehicle impeded *in vivo* bone regeneration in both MSC-seeded and acellular constructs. Although rMSC seeding was observed to enhance the osteoinductive potential of bone morphogenetic protein 2 (BMP-2)-containing constructs *in vitro*, co-delivery of rMSC and BMP-2 to the femoral defect space attenuated bone repair *in vivo* compared to BMP-2 delivery alone. Overall, despite *in vitro* evidence to the contrary, the present study observed no beneficial effects of these delivery strategies on cell-based bone tissue repair.

1. Introduction

Despite bone's innate ability to regenerate and remodel, large bone defects represent a significant clinical challenge [1, 2]. Critically-sized injuries, arising from incidences of trauma or bone resection, will, by definition, lead to non-union without therapeutic intervention [3]. Grafting of autologous tissue has several disadvantages that preclude its utility for large bone defect treatment, including limited tissue availability, donor-site morbidity, and prolonged surgical time [4-7]. Allografts represent a plausible alternative, but have shown difficulty with re-vascularization upon implantation and potential for subsequent fracture [8-10].

Limitations of grafting techniques have motivated the development of cell- and protein-based approaches. Bone morphogenetic proteins, first identified as osteoinductive factors in the 1960s, are clinically approved for the treatment of bone defects [11-15]. However, supraphysiological dosing of rhBMP-2, as often necessitated to ensure successful outcomes in treatment of critically-sized bone injuries, can have adverse side effects, including ectopic mineralization, inflammation, and bone resorption [16-24]. Furthermore, acellular treatments rely on the migration and subsequent differentiation of endogenous osteoprogenitor cells, the availability and accessibility of which is compromised in several patient populations [1, 25-31].

Therefore cell-based approaches may offer some advantages over the presentation of an osteoinductive cue alone. Delivered stem cells have the capacity to contribute both directly and indirectly to bone formation [32, 33]. In particular, treatment with mesenchymal stem cells (MSCs) has been shown to augment both fracture and large bone defect repair [2, 34-44]. However, while MSC-based bone repair approaches hold promise, development of a delivery strategy that produces clinically consistent results has not been established [45-47]. The long-term viability of cell-seeded, large volume implants has proven difficult to maintain and optimal

delivery parameters, including cell and vehicle properties, have yet to be determined [33, 41, 48-56].

The repair of bone tissue is strongly influenced by its local inflammatory environment, with injury stimulating an array of inflammatory signaling cascades [57, 58]. For this reason, one way to improve the potency of MSC-based therapeutics may be through manipulation of immunomodulatory factors secreted by the cells. Studies have highlighted the unique temporal role of factors and cytokines, such as tumor necrosis factor alpha (TNF-α), interleukin 6 (IL-6), and prostaglandin E_2 (PGE2), during bone tissue regeneration [58-61]. Although MSCs have inherent anti-inflammatory properties, recent work has found that this immunomodulatory potential can be enhanced by formation of MSCs into three-dimensional aggregates [62-65]. In particular, spheroid culture has been shown to increase production of immunomodulatory factors, including tumor necrosis factor-inducible gene 6 protein (TSG-6), indoleamine 2,3-dioxygenase (IDO), IL-6, and PGE2, in comparison to MSCs cultured in monolayer [64, 65]. Additionally, the exposure of MSC spheroids to pro-inflammatory cytokines, as found within injured tissue, further enhanced immunomodulatory factor secretion [64].

Aside from enriched anti-inflammatory capacity, MSC spheroids have demonstrated superior survival as well as angiogenic and osteogenic potential. Association of MSCs as spheroids has been found to decrease the extent of cell apoptosis and increase angiogenic factor expression *in vitro* [66, 67]. The delivery of aggregates to ischemic tissue has improved cell grafting, vasculature, and regenerative outcome [66-69]. In comparison to dissociated MSCs, cell aggregates exhibit improved osteogenic potential *in vitro* and *in vivo* [66, 70, 71]. However, although delivery of MSC aggregates demonstrated efficacy within a calvarial defect model, the ability of MSC spheroids to enhance bone regeneration has not been tested within a large

volume, critically-sized bone injury [70, 72].

Perfluorocarbon addition to cell-seeded constructs has previously been shown to potentiate survival [73-75]. Therefore, inclusion of the synthetic oxygen carrier perfluorotributylamine (PFTBA) as a means to better maintain delivered MSC viability either independent from or in conjunction with aggregate treatment was also of interest in this study. Oxygen solubility in PFTBA is 35 mM as compared to a concentration of 2.2 mM in water. Within hydrogel matrix, a co-delivered oxygen carrier can release O_2 into the surroundings and then reload itself by picking up oxygen from the plasma. The presence of 10% PFTBA has been shown to increase cellular metabolic activity in cell constructs *in vitro* compared to alginate gel alone [76]. In the aforementioned study, PFTBA buffered the drop in cellular metabolic activity normally seen upon encapsulation. The authors also approximated the theoretical maximum concentration of dissolved oxygen for a 1% alginate solution with 10% PFTBA as 49.1 mM for a 20% oxygen environment (tissue culture) and 12.1 mM for 5% O_2 [76]. Based on these values, cells within the PFTBA containing gel would not be expected to experience hypoxia upon initial implantation.

The objective of this work was to evaluate the effects of MSC aggregation as well as BMP-2 and PFTBA co-delivery on cell survival and cell-based bone regeneration in a large orthotopic defect model. We hypothesized that such delivery strategies of aggregation and oxygen carrier incorporation would augment bone repair in comparison to acellular or single cell-seeded therapeutics. To test this hypothesis, we evaluated the effects of these strategies using a multicomponent (hydrogel and mesh) carrier system delivered subcutaneously or to critically-sized femoral defects within both immunocompromised and syngeneic rodent models.

2. Experimental

2.1. MSC Culture and Aggregate Formation

For use in the immunocompromised rodent model, bone marrow-derived human MSCs (hMSCs), previously characterized for multipotency, were purchased from the Texas A&M University Health Science Center and cultured as described [77]. Briefly, two donor cell lines were expanded in Minimum Essential Medium alpha (αMEM) containing 16% v/v fetal bovine serum (FBS; Atlanta Biologicals; Lawrenceville, GA) and 100 units/mL penicillin/100 μg/mL streptomycin/2 mM L-glutamine (PSL; Invitrogen; Carlsbad, CA) at 37 ºC and 5% CO_2. At passage 2, cells were detached using 0.25% trypsin-EDTA (Invitrogen) and combined 1:1 to form a pooled hMSC population. In preparation for syngeneic delivery studies, previously characterized Lewis rat MSCs (rMSCs) were purchased (Sciencell Research Laboratories; Carlsbad, CA) and expanded until passage 2 in similar culture conditions. Following expansion, MSCs to be used in bioluminescent imaging (BLI) studies were labeled via lentiviral co-transduction for constitutive expression of green fluorescent protein (GFP) and firefly luciferase (Luc), as previously reported [78, 79]. To produce MSC aggregates, cells were seeded in 400-μm agarose micro-wells as described previously [64, 80]. Briefly, MSCs were added to micro-well inserts, centrifuged for 5 minutes at 200 g, and left to form aggregates (500 cells/spheroid) for 16 hrs. To characterize rMSC aggregate secretion and intracellular alkaline phosphatase (ALP) activity, a modified version of the hMSC aggregate protocol was implemented [64]. Culture media (n=6) was collected at 24 hrs from equivalent numbers of cells, either adherent "2D" rMSCs (1,300 cells/cm^2) or as aggregates (0.3 x10^6 cells/100 mm dish) cultured on a rotary orbital shaker. Media concentrations of rat interleukin 6 (IL-6) and prostaglandin E_2 (PGE2) were measured by ELISA assays (R&D Systems; Minneapolis, MN) and normalized to DNA

content quantified via the Quant-iT PicoGreen dsDNA Kit (Molecular Probes; Eugene, OR). ALP activity (n=6) was measured by incubation of cellular lysate in 20mM phosphatase substrate (p-NPP; Sigma-Aldrich; St. Louis, MO).

2.2. Alginate Embedding of hMSCs

Preceding work had demonstrated improved efficacy of large bone defect therapeutics with use of a carrier system, particularly that of RGD-functionalized alginate hydrogel [41, 81]. Thus, in the presently discussed study, hMSCs were embedded within RGD-functionalized alginate hydrogel (2% w/v; FMC BioPolymer; Ewing, NJ) in either single cell or aggregate form using a dual-syringe mixing technique with subsequent calcium sulfate (8.4 mg/mL; Sigma-Aldrich) cross-linking [77]. To verify maintenance of cell viability and spheroid structure following alginate incorporation and syringe injection, hMSC aggregates were embedded at densities of 0.5 and 2.0 $x10^6$ cells/150 μL and injected through a 20-gauge needle (n=3). Resultant hydrogel was stained using a LIVE/DEAD Kit (Invitrogen) and imaged using an inverted microscope (Axio Observer; Carl Zeiss; Thornwood, NY). To evaluate the correlation between BLI signal and cell number, individual and aggregated GFP/Luc hMSCs were embedded at densities of 0, 0.5, and 1.0 $x10^6$ cells/150 μL (n=6) and imaged using an IVIS Lumina machine (Caliper Life Sciences; Hopkinton, MA). Beetle luciferin (Fisher Scientific; Hampton, NH) was added to the culture media (0.21 mg/mL) 20 minutes prior to image acquisition (5 second exposure; 12.5 cm field of view). Living Image software version 3.2 (Caliper Life Sciences) was used to demarcate a circular region of interest (ROI) centered over each well and BLI counts were normalized to exposure time and ROI area. A subset of aggregate-seeded hydrogels (n=3) were cultured over 1 week, snap frozen in a hexane chilling

bath, sectioned using a CryoStar NX70 cryostat (Fisher Scientific), stained for lactate dehydrogenase (LDH) activity, and imaged using bright-field microscopy (Zeiss) [82].

2.3. Alginate Embedding of rMSCs

rMSC single cells or aggregates were similarly embedded within alginate hydrogel (2% w/v) along with added PBS (control) or perfluorotributylamine (10% w/v; PFTBA; Sigma-Aldrich) emulsion. Emulsions were prepared by sonication of PFTBA and phosphate-buffered saline (PBS; 2:3 ratio) or PBS alone with Lipoid E 80 (0.1 g/mL; Lipoid; Newark, NJ) using a Vibra-Cell VCX130PB sonicator (Sonics & Materials; Newtown, CT) for 2 minutes at 31% amplitude. Prior to alginate cross-linking, all rMSC groups and associated acellular controls received identical emulsion concentrations to produce 0% and 10% PFTBA hydrogels. GFP/Luc rMSC-seeded alginate with single or aggregated cells (0.5 $x10^6$ cells/150 μL) and 0% or 10% PFTBA was injected into electrospun, polycaprolactone (PCL) mesh tubes (150 μL/construct) and cultured over 4 days under hypoxic conditions (3% O_2). To quantify change in viable cell number, longitudinal BLI was performed on Days 0, 2, and 4 using the protocol described in sub-section 2.2 (n=8) with culture media (2 mL/well) replaced following each timepoint. In preparation for segmental defect delivery, single cell or aggregated rMSCs were seeded at a density of 0 (acellular) or 1.0 $x10^6$ cells/150 μL, with or without PFTBA, and recombinant human BMP-2 (1.5 μg/150 μL; rhBMP-2). Resultant hydrogels (n=4) were cultured in mesh tubes with media collected and replaced on Days 1, 4, and 7. Conditioned media were measured for BMP-2 content using an ELISA assay (R&D Systems) and BMP-2 functional activity examined using a previously established ALP induction protocol [83, 84]. Briefly, mouse clonal pre-osteoblasts (MC3T3-E1; American Type Culture Collection; Manassas, VA) were plated at confluence (1,300 cells/cm^2) and cultured in the construct-conditioned media. After 3 days,

MC3T3-E1 cells were washed, fixed, and incubated in 7.6mM p-NPP to determine ALP activity. Normalized ALP activity was calculated using DNA content, measured as previously described in sub-section 2.1.

2.4. Subcutaneous Implantation

Surgical implantation was conducted in accordance with the Georgia Institute of Technology approved IACUC protocol #A13023, as described previously [77]. Delivered hydrogel volume and cell dose were selected based on data collected during model system development and examination of MSC survival as a function of delivered single cell dose [85-87]. Alginate hydrogel seeded with single cell or aggregated GFP/Luc hMSCs at a density of 0.5 $x10^6$ cells/150 μL (n=5) were maintained at 4 °C for 1-4 hrs prior to delivery, at which point the hydrogel was injected into PCL tubes (150 μL/construct) and implanted within 11-week-old female, athymic nude rats (Charles River Labs; Wilmington, MA). As previously described, two dorsal incisions were made to prepare four subcutaneous pockets per animal. For syngeneic delivery studies, rMSC-seeded hydrogels were similarly implanted within 11-week-old male, inbred Lewis rats (Harlan Laboratories; Indianapolis, IN). GFP/Luc and unlabeled rMSCs were combined at a 2:1 ratio prior to alginate embedding. Constructs containing single cell or aggregated rMSCs (0.5 $x10^6$ cells/150 μL) and with or without PFTBA were delivered alongside acellular controls (n=7-10).

2.5. Subcutaneous BLI, Vascular, and Histological Analyses

Nude rats underwent longitudinal BLI at Days 0, 1, 3, 5, 7, and 14 post-operatively using a previously established protocol [77]. Anesthetized rats received a subcutaneous injection of 300 μL luciferin (21 mg/mL in saline) at a distance of 2-4 mm from each construct site. The animals were scanned on either side 30 minutes post luciferin injection (10 second exposure;

12.5 cm field of view) and images were evaluated using a 4 cm^2 elliptical ROI. Following BLI measures on Day 14, nude rats underwent vascular perfusion using serially applied saline (0.9% w/v), papaverine hydrochloride (0.4% w/v in saline), neutral buffered formalin (10% v/v), and the radiopaque contrast agent Microfil (Flow Tech; Carver, MA) solutions. Explants were excised and imaged via microcomputed tomography (μCT) scans on a MicroCT42 (Scanco Medical; Brüttisellen, Switzerland) at 55k Vp, 145 μA, and a 12 μm voxel size. Acquired slices were contoured and segmented using a low-pass Gaussian filter (sigma=1.2, support=2) to evaluate vascular volume within the construct interior alone. Following μCT scans, explants were paraffin embedded, sectioned via microtome (Microm; Walldorf, Germany), stained with Masson's trichrome or human nuclear mitotic apparatus protein 1 (NuMA), and imaged (Zeiss). For NuMA immunohistochemistry, sections were deparaffinized, rehydrated, subjected to antigen retrieval (sodium citrate buffer pH= 6, 95 °C, 20 min) and incubated in 3% hydrogen peroxide (to block endogenous peroxidase activity) for 10 min before blocking for 30 min in 2% BSA [88]. Sections were incubated in either primary antibody solution (NuMA (1:100, ab97585, Abcam) or in non-immune serum control. Secondary antibody coupled to horseradish peroxidase (Vector Labs) was then applied. Color development was performed with diaminobenzidine (Sigma) for 10 seconds before methyl green counterstaining and mounting in Cytoseal (Thermo Scientific). Human and rat tissue sections were used as positive and negative control tissues, respectively.

Lewis rats underwent similar examination with longitudinal BLI performed on Days 0, 1, 7, and 14; followed by takedown for vascular and histological analyses on Day 14. These samples were evaluated for tissue development and delivered rMSC retention via Hematoxylin and Eosin (H&E) and DAPI staining. To examine delivered cell hypoxia, HIF-1 alpha

immunostaining was conducted with the following protocol validation and application methods described. hMSCs were grown in chamber slides, subjected to 0-150 μM desferoxamine (DFO) for 24 hrs, fixed in 4% formaldehyde in PBS for 10 minutes, washed in PBS, and air dried. A 1% BSA/10% normal donkey serum/0.3M glycine in 0.1% PBS-Tween solution was applied for 1 hr to permeabilize and block the cells before incubation with rabbit polyclonal 1/100 anti HIF-1 alpha antibody (ab2185, Abcam) for 1 hr at room temperature (RT). After washing, slides were incubated with donkey anti-rabbit Dylight 594 (Thermo Scientific) for 1 hr at RT before nuclear counterstaining with DAPI. For tissue samples, sections were baked, deparaffinized, subjected to 2 % sodium borohydride in PBS for 30 minutes (to reduce autofluorescence), permeabilized, blocked, and treated with primary antibody. The subsequently applied secondary antibody was conjugated to Dylight 488 (Thermo Scientific) since delivered rMSCs were already labeled with DiI (rhodamine).

2.6. Segmental Defect Implantation

Segmental defect surgeries were conducted in accordance with the Georgia Institute of Technology approved IACUC protocol #A14037. Due to a lengthened surgical timeline in comparison to subcutaneous implantation, the effect of 4 °C syringe incubation on alginate-embedded MSC viability was examined prior to delivery. Single cell or aggregated MSCs at 1.0 $x10^6$ cells/150 μL alginate (n=3) were incubated for 0, 4, or 8 hrs at 4 °C and subsequently injected, stained via LIVE/DEAD Kit (Invitrogen), and imaged (Zeiss). rMSC-seeded hydrogels containing emulsions were analyzed using a cell metabolic assay (n=3) due to imaging challenges resulting from altered gel opacity. Single cell or aggregated rMSC-seeded hydrogels containing no additive, PBS, or PFTBA emulsion and having undergone a 0- or 8-hr syringe

incubation at 4 °C, were cultured for 48 hrs and assessed by CellTiter-Blue viability assay (Promega; Madison, WI) according to the manufacturer's instructions. On each date of surgery, bilateral femoral defects were created in 13-week-old rats as previously described [87, 89]. Briefly, an 8-mm critically-sized defect was created in the mid-diaphysis of each femur, following attachment of a polysulfone fixation plate to provide limb stabilization. Injuries were treated with a PCL mesh surrounding each defect followed by injection of alginate hydrogel (150 μL), incubated for 1-8 hrs at 4°C prior to delivery. Nude rats received acellular, single cell, or aggregated hMSC-seeded (1.0 x10^6 cells/150 μL) alginate containing a 2-μg dose of rhBMP-2 (n=7-10). A treatment group containing hMSC aggregate-seeded alginate without rhBMP-2 was also included. Lewis rat defects were treated with acellular, single cell, or aggregated rMSC-seeded (1.0 x10^6 cells/150 μL) alginate containing PBS or PFTBA emulsion and a 1.5-μg dose of rhBMP-2 (n=6-9). A subset of Lewis rat defects received rMSCs labeled with DiI stain (Invitrogen) to facilitate downstream histological analysis.

2.7. Segmental Defect Radiography and μCT Analyses

Longitudinal bone regeneration for all rats was assessed qualitatively via radiography (Faxitron MX-20 Digital; Faxitron Bioptics; Tucson, AZ) at 4, 8, and 12 weeks post-operatively. At the same timepoints, nude rats also received quantitative evaluation of bone formation by μCT (VivaCT40; Scanco Medical) at 55 kVp, 145 μA, and a 38.9 μm voxel size (n=7-10). Regenerated bone volume was analyzed using a volume of interest (VOI) consisting of 100 slices within the defect center. Lewis rats received *ex vivo* μCT evaluation due to their prohibitive size. Explanted femurs were scanned at 55 kVp, 145 μA, and a 21 μm voxel size then evaluated using a VOI consisting of 280 slices (n=6-9).

2.8. Segmental Defect Biomechanical and Histological Analyses

Femurs were explanted at 12 week post-operatively and underwent torsional testing to failure as previously reported [87]. Briefly, bone ends were potted in Wood's metal (Alfa Aesar; Ward Hill, MA) following soft tissue and fixation plate removal. Using an ELF 3200 machine (Bose ElectroForce Systems Group; Eden Prairie, MN), samples were displaced at 3 °/s. Maximum torque and torsional stiffness were calculated for the nude (n=5-7) and Lewis (n=6-9) rat explants. Following biomechanical testing, Lewis rat defects were removed, decalcified (Cal-ExII; Fisher Scientific), and paraffin embedded. Sectioned samples were imaged (Zeiss) following staining with Safranin O (SafO), DAPI, or pan macrophage marker (CD68). For CD68 immunohistochemistry, sections were deparaffinized, rehydrated, permeabilized (0.2% Triton X-100 in PBS for 10 min), and blocked in 5% donkey serum for 30 min. Sections were then incubated in CD68 antibody (1:100, MCA341, AbD Serotec) or in blocking solution alone in a humid chamber overnight at 4°C before exposure to secondary antibody (donkey anti mouse IgG Alexa 488, ThermoFisher Scientific) and DAPI counterstaining.

2.9. Statistical Analysis

Values are displayed as mean +/- standard error of mean (SEM) unless otherwise stated with statistical significance defined by $p<0.05$. Data were analyzed using two-way analyses of variance (ANOVA) with Tukey post hoc comparisons within the Minitab software (State College, PA).

3. Results and Discussion

3.1. Subcutaneous Implantation of hMSC Aggregates in Nude Rats

Aggregation of MSCs can upregulate immunomodulatory mediators, engineering the cell

secretome towards a pro-angiogenic and anti-inflammatory phenotype. Due to the interplay of regenerating bone tissue with its inflammatory and vascular milieu, MSC aggregation was pursued as an approach to augment cell-based bone defect repair [57, 90, 91]. Using an immunocompromised rodent model, the effect of hMSC aggregation on cell survival and construct vasculature was first explored via a subcutaneous implantation study. Subsequently, the capacity of delivered hMSC spheroids to facilitate low dose BMP-2-mediated bone regeneration was evaluated within a critically-sized femoral defect.

In preparation for *in vivo* delivery, *in vitro* characterization of hMSC aggregates incorporated into RGD-alginate hydrogels was performed. It was found that hMSCs aggregates maintained their viability and structure following the alginate cross-linking and syringe injection procedures (Fig. 1A). Correlation of bioluminescent imaging (BLI) signal vs. viable cell number for GFP/Luc hMSC aggregates was observed to be linear ($r^2 = 0.75$) and statistically similar to that of GFP/Luc hMSCs embedded as single cells (Fig. 1B). Culture of these constructs over 1 week illustrated the loss of original hMSC aggregate structure within the peptide modified alginate hydrogel (Fig. 1C).

Alginate/mesh constructs seeded with single cell or aggregated GFP/Luc hMSCs were implanted subcutaneously in nude rats and monitored for cell survival via BLI. hMSC aggregation had no adverse effect on viable cell number, but both groups exhibited low (1-2%) survival through 14 days post-operatively (Fig. 1D-E). On Day 14, vascular perfusion and histological analyses were performed to examine tissue development contiguous to the constructs. There was no effect of aggregate delivery on construct vascular volume (Fig. 1F) or gross vessel morphology, as assessed qualitatively via representative μCT vasculature reconstructions (Fig. 1G). Masson's trichrome staining revealed the presence of extracellular

matrix (ECM) formation both between fragments of residual alginate hydrogel (yellow arrows) and within the hydrogel fragments associated with the implanted single and aggregated cells (green arrows) (Fig. 1H). The morphology of ECM regions embedded within the alginate fragments was observed to be qualitatively distinct between the treatment groups, with single cell delivery resulting in a more even distribution of pockets throughout the construct. In contrast, aggregate-seeded samples had a more heterogeneous distribution of ECM formation, including regions that appeared to be branching (red arrows) or multi-nodal (pink arrows). NuMA staining found that the aggregate delivery resulted in greater fragmentation of the alginate gel as the aggregates broke down, whereas the single cells remained trapped in the alginate at 14 days post implantation (Fig. 1I).

3.2. hMSC Aggregation for Large Bone Defect Repair in Nude Rats

To examine the effect of hMSC aggregation on cell-based bone regeneration, bilateral critically-sized defects were created in nude rats and treated with alginate/mesh constructs containing a 2-μg dose of BMP-2 and no cells, single cells, or aggregated hMSCs. An additional aggregate group without BMP-2 was delivered to observe the extent of aggregate-mediated bone defect repair in the absence of co-delivered osteoinductive stimulus. Longitudinal *in vivo* μCT at 4, 8, and 12 weeks post-operatively revealed no difference in regenerated bone volume across BMP-2-containing treatments (Fig. 2A). However, little to no bone formation was observed in the groups without BMP-2. Biomechanical testing data was more variable than regenerated bone volume results, with no significant effect of hMSC delivery or BMP-2 dose on maximum torque (Fig. 2B) or torsional stiffness (Fig. 2C) measurements.

Statistical analysis of the regenerated bone volume via two-way ANOVA revealed a

significant effect of animal (p=0.021), but not treatment (p=0.768), for nude rats receiving bilateral BMP-2-containing treatments (data not shown). In the nude rat model biological variability was found to be a significant predictor of regenerative outcome. This finding motivated the continuation of aggregate delivery studies within a syngeneic animal model (Lewis rats), given that significant animal-to-animal variability had not been observed in previous studies using immunocompetent rat strains (data not shown).

3.3. *In Vitro* Characterization of rMSC Aggregates

In transitioning to the syngeneic model, *in vitro* characterization of rMSC spheroid immunomodulatory properties was first conducted. The same protocol employed for hMSC aggregate formation was effective in producing rMSC aggregates. Spheroids formed over 16 hrs when rMSCs were seeded in agarose micro-wells (Fig. 3A). Up-regulated immunomodulatory factor secretion, as previously observed for hMSCs spheroids, occurred with aggregation of rMSCs as well. rMSC aggregates exhibited increased production of IL-6 and PGE2 over 24 hrs in comparison to cells plated in 2D (Fig. 3B). Additionally, intracellular ALP activity was enhanced by rMSC aggregation (Fig. 3C).

Therefore, rMSC aggregation increased the secretion of IL-6 and PGE2 factors [64] consistent with hMSC findings. Interestingly, aggregation also enhanced rMSC intracellular ALP activity. Although a known characteristic of MSC aggregates cultured under osteoinductive conditions, this had not previously investigated in the absence of a differentiation stimulus [66, 70, 71, 92]. Overall, similarities in the effect of MSC aggregation across cell species afforded pre-clinical relevance to testing spheroid delivery within the syngeneic rodent model.

3.4. *In Vitro* Use of Synthetic Oxygen Carrier for rMSC Delivery

Motivated by the low survival rate achieved with hMSC delivery (Fig. 1D), the effect of co-delivered PFTBA, a synthetic oxygen carrier, was explored for rMSC implantation. In preparation for *in vivo* delivery, the effect of PFTBA addition (10% w/v) to alginate/mesh constructs on embedded GFP/Luc rMSC survival was investigated *in vitro* under hypoxic conditions (3% O_2). Quantification of viable cell number via BLI measurement (normalized to Day 0) found improved maintenance of rMSC viability for single cell (SC) groups and no effect of PFTBA addition through 4 days (Fig. 3D). As differences exist between *in vitro* and *in vivo* hypoxic environments and given the finding that PFTBA co-delivery had no negative effect on embedded-rMSC viability, use of PFTBA was continued in subsequent experiments.

3.5. Subcutaneous Implantation of rMSC Aggregates in Lewis Rats

Single cell (SC) and aggregate (AG) seeded in alginate/mesh constructs either with (+) or without (-) PFTBA, as well as acellular (Acell) controls, were implanted subcutaneously in Lewis rats and monitored via BLI. Normalized BLI measurement over 14 days post-implantation demonstrated a significant overall effect of cell presentation ($p_{SCvs.AG}$=0.009), but not PFTBA incorporation (p_{PFTBA}=0.075), on *in vivo* survival (Fig. 4A). Single rMSC delivery in the absence of PFTBA (SC-) resulted in the greatest viable cell number on Day 1 post-operatively and displayed a high degree of variability, with several samples exhibiting a marked increase in viable cell number between Days 0 and 1. Despite early differences in viability, representative heatmaps illustrate a qualitative decrease in BLI signal for all rMSC delivery groups by Day 14 (Fig. 4B). Interestingly, although the majority of acellular implants displayed negligible BLI signal throughout the study duration, several Acell- constructs increased in BLI signal over time

(data not shown). This phenomenon had not been observed in former hMSC delivery experiments and was not, in the present study, correlated to the BLI signal recorded from adjacent rMSC-seeded constructs. A lack of correlation suggested that, for a given rMSC-seeded construct, live cell retention and loss due to migration were not proportionally related.

Examining tissue composition within the subcutaneous explants, there were qualitative differences in the size and distribution of construct vasculature across experimental groups (Fig. 4C). However, upon quantification, neither rMSC nor PFTBA delivery strategy had an independent effect on construct vascular volume (Fig. 4D). In comparing individual treatment groups, single rMSC seeded constructs without PFTBA (SC-) contained more vasculature than acellular, PFTBA-containing (Acell+) constructs. Histological examination via Hematoxylin and Eosin staining revealed a similar extent of residual alginate pieces surrounded by granulation tissue across all experimental groups (Fig. 4E). Consistent with bioluminescent data, fluorescence microscopy confirmed the retention of a delivered rMSC population within constructs initially seeded with single and aggregated cells (Fig. 4F). Aggregation may have promoted rMSC migration, as evidenced by single cell retention within the alginate pieces through 14 days while rMSCs delivered as spheroids displayed increased separation over time, indicative of cell movement.

Under normoxic conditions, the half-life of the HIF-1 alpha subunit is short and as such it is mainly undetectable in cells or tissues under these conditions. It becomes stabilized as oxygen concentrations approach 5% or below and this causes translocation to the nucleus. Therefore, presence of this subunit in the nucleus implies that the cell is experiencing hypoxia. Based on HIF-1 alpha immunostaining of the Day 14 explants, hypoxia within alginate-containing areas was observed to the same extent in aggregates with or without co-delivered PFTBA (Fig. 4H).

Therefore, at least for the aggregates, it does not appear that PFTBA inclusion had any positive effect on hypoxia. For the single cell groups, with the caveat that there were fewer labeled cells present at 14 days post implantation, there appeared to be qualitatively fewer hypoxic cells in the samples containing PFTBA. The reduced hypoxic cell number with PFTBA addition could be attributed to the oxygen carrier having a positive influence on hypoxia in the single cell group. This positive effect of PFTBA on delivered single cells, but not the aggregate-seeded constructs, may potentially be due to the carrier's ability to exert a meaningful effect on a less dense population of cells. In this way, we have observed differences in the cellular response to PFTBA co-delivery based on aggregate vs. single cell delivery.

Although perfluorocarbon addition to cell-seeded constructs has previously been shown to potentiate survival, our study did not observe this retention of viable rMSCs when tested under hypoxic culture or subcutaneously [73-75]. Given the transport limitations imposed by our large volume alginate/mesh construct, it is possible that the effect of perfluorocarbon incorporation was indiscernible experimentally [93]. However, PFTBA incorporation facilitated a short-term enhancement of osteoinductive factor release *in vitro*, as examined using a differentiation assay performed on pre-osteoblasts (Fig. 5).

3.6. Release of BMP-2 from rMSC-Seeded Constructs *In Vitro*

In preparation for implantation in the segmental defect model, the effect of rMSC and PFTBA incorporation on co-delivered BMP-2 release was quantified *in vitro*. Alginate/mesh constructs were prepared with no (Acell), single cell (SC), or aggregated (AG) rMSCs, with (+) or without (-) PFTBA, and a 1.5-μg dose of BMP-2. Conditioned media were collected from cultured constructs on Days 1, 4, and 7 to measure (i) BMP-2 content and (ii) BMP-2 functional

activity by induction of ALP activity in a pre-osteoblast cell line (MC3T3-E1). Over the first 24 hours of culture, constructs across all groups released comparable amounts of BMP-2 (Fig. 5A). However, following this initial period, more BMP-2 was released from acellular constructs than those seeded with single ($p=0.002$) or aggregated ($p=0.046$) rMSCs. No effect of PFTBA incorporation was observed at any point in time. In contrast to BMP-2 release data, the presence of rMSCs considerably enriched the induction capacity of conditioned media on pre-osteoblast ALP activity (Fig. 5B). Specifically, ALP activity of MC3T3-E1 cells treated with conditioned media from the first 24 hrs of construct culture was increased with rMSC-seeding and PFTBA addition. At all timepoints, media conditioned by aggregate-seeded constructs were most effective in inducing ALP activity. This increased osteogenic potential was especially notable given that the acellular constructs released more BMP-2, suggesting that either the osteogenic protein released from acellular scaffolds was less active or that additional morphogens released by the aggregate-seeded constructs were contributing to MC3T3-E1 differentiation. To determine whether changes in induction capacity were attributed solely to MC3T3-E1 number, ALP activity was normalized to DNA content. Normalized data continued to show a benefit of rMSC and PFTBA delivery, indicating that enhancement of total ALP activity was not simply due to growth of MC3T3-E1 cells.

The heightened osteoinductive factor release, seen with embedded rMSC aggregates, may be attributable to a number of secreted factors acting in isolation or synergistically to promote differentiation. rMSC spheroids have been reported to release fibroblast growth factor (FGF) and to decrease dickkopf 1 (Dkk-1) production, each serving to facilitate osteoblast differentiation [94-97]. Although enhanced expression of PGE2 and IL-6 motivated the evaluation of aggregation for MSC-based bone repair, the osteoinductive effect observed in this assay was

likely not due to these anti-inflammatory factors. IL-6 is shown to reduce ALP activity in MC3T3-E1 cells and PGE2 is considered to impact bone repair predominantly via immune cell signaling [58, 98, 99]. In fact, similar to IL-6 expression, aggregate-driven PGE2 signaling may have also acted against the observed effect, as increased PGE2 concentration is associated with a decrease in MC3T3-E1 ALP activity [100-102]. In all, these promising *in vitro* results prompted investigation of the rMSC aggregation strategy within a bone defect model.

3.7. rMSC Aggregate Delivery for Bone Defect Repair in Lewis Rats

To examine the effect of rMSC aggregation on cell-mediated bone regeneration, bilateral femoral defects created in Lewis rats were treated with alginate/mesh constructs containing a 1.5-μg dose of BMP-2, seeded with no cells, single cells, or aggregated rMSCs, alone or with 10% PFTBA. Longitudinal radiographs captured at 4, 8, and 12 weeks post-operatively showed qualitatively less bone regeneration with rMSC or PFTBA delivery (data not shown). In fact, only injuries treated with acellular constructs lacking PFTBA (Acell-) demonstrated defect bridging. Treated femurs were explanted and analyzed via μCT and torsional testing at 12 weeks. Representative mineral density heatmaps were consistent with radiograph observations, showing a qualitative attenuation of bone repair with rMSC or PFTBA delivery (Fig. 6A). Quantification of regenerated bone tissue properties revealed that bone volume was greatest with Acell- treatment and that rMSC or PFTBA addition attenuated regenerated bone volume in both an individual and additive manner (Fig 6B). Functional restoration of tissue function was accomplished to the greatest extent with Acell- treatment, as assessed by measurement of maximum torque (Fig. 6C) and torsional stiffness (Fig. 6D). The addition of rMSCs or PFTBA resulted in lower levels in either biomechanical metric.

Tissue development within the defect space was examined histologically using a Safranin O stain (SafO stains alginate pink/orange) and found to be consistent with μCT analysis (Fig. 6E). In the absence of rMSC or PFTBA delivery (Acell-), defects at 12 weeks contained organized bone tissue surrounding pieces of mineralized alginate. With the addition of cells or co-delivered PFTBA, mineralized tissue within the defect space was qualitatively reduced and the amount of residual alginate increased. Fluorescence microscopy revealed that all rMSC-treated defects contained DiI signal present at 12 weeks, suggesting persistence of delivered cells through the study conclusion (Fig. 6F). Although of diminished intensity, DiI signal was detected in the injury space of acellular-treated defects as well, yet only for samples extracted from rats receiving rMSC treatment in the contralateral limb (data not shown). The fluorescent signal was co-localized to regions of CD68 staining, suggesting that the DiI label may have trafficked from the contralateral limb via macrophages.

Interestingly, the addition of PFTBA to alginate/mesh constructs was found to impede bone regeneration irrespective of co-delivered rMSCs. PFTBA has previously been shown to improve cell-based mineralization, but it had not been evaluated for its impact on an acellular treatment strategy [73-75]. As PFTBA incorporation had no discernible effect on the amount of BMP-2 released *in vitro*, we speculate that PFTBA-attenuated bone repair *in vivo* may have been due to differential release kinetics or the consequence of modified alginate matrix properties, potentially perturbing the migration of endogenous cells into the defect region due to altered release kinetics [103].

4. Conclusions

Despite the promising effect of rMSC-seeding, either as single or aggregated cells, on the osteoinductive capacity of construct-released factors *in vitro*, cell delivery attenuated BMP-2 mediated bone defect repair when challenged *in vivo*. In addition, within the studies presented here, cell aggregation or use of an oxygen carrier did not improve cell survival or augment bone regeneration *in vivo* despite encouraging results in culture. Co-delivery of cells with BMP reduced overall BMP release *in vitro* and the same effect was seen in the bone defect studies, suggesting that co-delivery of cells decreases the effectiveness of BMP delivery. Interestingly, the presence of some intact human nuclei was detected in and around alginate hydrogel 14 days post implantation in the subcutaneous nude rat model and the presence of small clusters of DiI-labeled rat MSCs was seen out to 12 weeks in the rat bone defect model. Future work will concentrate on strategies to further improve survival of implanted cells in subcutaneous and bone defect models.

5. Acknowledgements

This study was supported by grants from the Center for Advanced Bioengineering Soldier Survivability (CABSS), Armed Forces Institute of Regenerative Medicine (AFIRM), and the 2014 Robert M. Nerem International Travel Award. Emily Butts, Albert Cheng, Laura Cox, Marian Hettiaratchi, Brett Klosterhoff, Laxminarayanan Krishnan, Angela Lin, Lauren Priddy, David Reece, Marissa Ruehle, Giuliana Salazar-Noratto, Nick Servies, Sanjay Sridaran, Brennan Torstrick, Nick Willett, and Boao Xia assisted with surgical procedures.

6. Notes and References

1. Calori, G.M., et al., *The use of bone-graft substitutes in large bone defects: any specific needs?* Injury, 2011. **42 Suppl 2**: p. S56-63.

2. Zhang, Z.Y., et al., *The potential of human fetal mesenchymal stem cells for off-the-shelf bone tissue engineering application.* Biomaterials, 2012. **33**(9): p. 2656-72.

3. Johnson, E.E., M.R. Urist, and G.A. Finerman, *Resistant nonunions and partial or complete segmental defects of long bones. Treatment with implants of a composite of human bone morphogenetic protein (BMP) and autolyzed, antigen-extracted, allogeneic (AAA) bone.* Clin Orthop Relat Res, 1992(277): p. 229-37.

4. Younger, E.M. and M.W. Chapman, *Morbidity at bone graft donor sites.* J Orthop Trauma, 1989. **3**(3): p. 192-5.

5. Banwart, J.C., M.A. Asher, and R.S. Hassanein, *Iliac crest bone graft harvest donor site morbidity. A statistical evaluation.* Spine (Phila Pa 1976), 1995. **20**(9): p. 1055-60.

6. Goulet, J.A., et al., *Autogenous iliac crest bone graft. Complications and functional assessment.* Clin Orthop Relat Res, 1997(339): p. 76-81.

7. St John, T.A., et al., *Physical and monetary costs associated with autogenous bone graft harvesting.* Am J Orthop (Belle Mead NJ), 2003. **32**(1): p. 18-23.

8. Berrey, B.H., Jr., et al., *Fractures of allografts. Frequency, treatment, and end-results.* J Bone Joint Surg Am, 1990. **72**(6): p. 825-33.

9. Finkemeier, C.G., *Bone-grafting and bone-graft substitutes.* J Bone Joint Surg Am, 2002. **84-A**(3): p. 454-64.

10. Kim, S., et al., *TMPRSS4 induces invasion and epithelial-mesenchymal transition through upregulation of integrin alpha5 and its signaling pathways.* Carcinogenesis, 2010. **31**(4): p. 597-606.

11. Wozney, J.M., et al., *Novel regulators of bone formation: molecular clones and activities.* Science, 1988. **242**(4885): p. 1528-34.

12. Wang, E.A., et al., *Purification and characterization of other distinct bone-inducing factors.* Proc Natl Acad Sci U S A, 1988. **85**(24): p. 9484-8.

13. Gautschi, O.P., S.P. Frey, and R. Zellweger, *Bone morphogenetic proteins in clinical applications.* ANZ J Surg, 2007. **77**(8): p. 626-31.

14. Bessa, P.C., M. Casal, and R.L. Reis, *Bone morphogenetic proteins in tissue engineering: the road from laboratory to clinic, part II (BMP delivery).* J Tissue Eng Regen Med, 2008. **2**(2-3): p. 81-96.

15. Urist, M.R., *Bone: formation by autoinduction.* Science, 1965. **150**(3698): p. 893-9.

16. Giannoudis, P.V., T.A. Einhorn, and D. Marsh, *Fracture healing: a harmony of optimal biology and optimal fixation?* Injury, 2007. **38 Suppl 4**: p. S1-2.

17. Poynton, A.R. and J.M. Lane, *Safety profile for the clinical use of bone morphogenetic proteins in the spine.* Spine (Phila Pa 1976), 2002. **27**(16 Suppl 1): p. S40-8.

18. Lee, K.B., et al., *BMP induced inflammation: A comparison of rhBMP-7 and rhBMP-2.* J Orthop Res, 2012.

19. Benglis, D., M.Y. Wang, and A.D. Levi, *A comprehensive review of the safety profile of bone morphogenetic protein in spine surgery.* Neurosurgery, 2008. **62**(5 Suppl 2): p. ONS423-31; discussion ONS431.

20. Shields, L.B., et al., *Adverse effects associated with high-dose recombinant human bone morphogenetic protein-2 use in anterior cervical spine fusion.* Spine (Phila Pa 1976), 2006. **31**(5): p. 542-7.

21. Perri, B., et al., *Adverse swelling associated with use of rh-BMP-2 in anterior cervical discectomy and fusion: a case study.* Spine J, 2007. **7**(2): p. 235-9.

22. Smucker, J.D., et al., *Increased swelling complications associated with off-label usage of rhBMP-2 in the anterior cervical spine.* Spine (Phila Pa 1976), 2006. **31**(24): p. 2813-9.

23. Marsh, D.R. and G. Li, *The biology of fracture healing: optimising outcome.* Br Med Bull, 1999. **55**(4): p. 856-69.

24. Hollinger, J.O., et al., *Role of bone substitutes.* Clin Orthop Relat Res, 1996(324): p. 55-65.

25. Bruder, S.P. and B.S. Fox, *Tissue engineering of bone. Cell based strategies.* Clin Orthop Relat Res, 1999(367 Suppl): p. S68-83.

26. Sethe, S., A. Scutt, and A. Stolzing, *Aging of mesenchymal stem cells.* Ageing Res Rev, 2006. **5**(1): p. 91-116.

27. Fehrer, C. and G. Lepperdinger, *Mesenchymal stem cell aging.* Exp Gerontol, 2005. **40**(12): p. 926-30.

28. Cao, J., et al., *Photocatalytic activity of novel AgBr/WO3 composite photocatalyst under visible light irradiation for methyl orange degradation.* J Hazard Mater, 2011. **190**(1-3): p. 700-6.

29. Service, R.F., *Tissue engineers build new bone.* Science, 2000. **289**(5484): p. 1498-500.

30. Caplan, A.I., *Adult mesenchymal stem cells for tissue engineering versus regenerative medicine.* J Cell Physiol, 2007. **213**(2): p. 341-7.

31. Hutmacher, D.W. and S. Cool, *Concepts of scaffold-based tissue engineering--the rationale to use solid free-form fabrication techniques.* J Cell Mol Med, 2007. **11**(4): p. 654-69.

32. Maraldi, T., et al., *Human amniotic fluid stem cells seeded in fibroin scaffold produce in vivo mineralized matrix.* Tissue Eng Part A, 2011. **17**(21-22): p. 2833-43.

33. Waese, E.Y., R.A. Kandel, and W.L. Stanford, *Application of stem cells in bone repair.* Skeletal Radiol, 2008. **37**(7): p. 601-8.

34. Cao, L., et al., *The use of autologous enriched bone marrow MSCs to enhance osteoporotic bone defect repair in long-term estrogen deficient goats.* Biomaterials, 2012. **33**(20): p. 5076-84.

35. Dupont, K.M., et al., *Synthetic scaffold coating with adeno-associated virus encoding BMP2 to promote endogenous bone repair.* Cell Tissue Res, 2012. **347**(3): p. 575-88.

36. Jones, E. and X. Yang, *Mesenchymal stem cells and bone regeneration: current status.* Injury, 2011. **42**(6): p. 562-8.

37. Kadiyala, S., et al., *Culture expanded canine mesenchymal stem cells possess osteochondrogenic potential in vivo and in vitro.* Cell Transplant, 1997. **6**(2): p. 125-34.

38. Quarto, R., et al., *Repair of large bone defects with the use of autologous bone marrow stromal cells.* N Engl J Med, 2001. **344**(5): p. 385-6.

39. Dallari, D., et al., *In vivo study on the healing of bone defects treated with bone marrow stromal cells, platelet-rich plasma, and freeze-dried bone allografts, alone and in combination.* J Orthop Res, 2006. **24**(5): p. 877-88.

40. Nather, A., et al., *Effect of autologous mesenchymal stem cells on biological healing of allografts in critical-sized tibial defects simulated in adult rabbits.* Ann Acad Med Singapore, 2010. **39**(8): p. 599-606.

41. Dosier, C.R., et al., *Effect of cell origin and timing of delivery for stem cell-based bone tissue engineering using biologically functionalized hydrogels.* Tissue Eng Part A, 2015. **21**(1-2): p. 156-65.

42. Sheyn, D., et al., *Genetically Modified Mesenchymal Stem Cells Induce Mechanically Stable Posterior Spine Fusion.* Tissue Engineering Part A, 2010. **16**(12): p. 3679-3686.

43. Petite, H., et al., *Tissue-engineered bone regeneration.* Nat Biotechnol, 2000. **18**(9): p. 959-63.

44. Peters, A., et al., *Locally applied osteogenic predifferentiated progenitor cells are more effective than undifferentiated mesenchymal stem cells in the treatment of delayed bone healing.* Tissue Eng Part A, 2009. **15**(10): p. 2947-54.

45. Osugi, M., et al., *Conditioned media from mesenchymal stem cells enhanced bone regeneration in rat calvarial bone defects.* Tissue Eng Part A, 2012. **18**(13-14): p. 1479-89.

46. Bruder, S.P., et al., *Mesenchymal stem cells in osteobiology and applied bone regeneration.* Clin Orthop Relat Res, 1998(355 Suppl): p. S247-56.

47. Janicki, P. and G. Schmidmaier, *What should be the characteristics of the ideal bone graft substitute? Combining scaffolds with growth factors and/or stem cells.* Injury, 2011. **42 Suppl 2**: p. S77-81.

48. Grieshaber, S.E., et al., *Assembly Properties of an Alanine-Rich, Lysine-Containing Peptide and the Formation of Peptide/Polymer Hybrid Hydrogels.* Macromol Chem Phys, 2011. **212**(3): p. 229-239.

49. Ide, C., et al., *Bone marrow stromal cell transplantation for treatment of sub-acute spinal cord injury in the rat.* Brain Res, 2010. **1332**: p. 32-47.

50. Rustad, K.C., et al., *Enhancement of mesenchymal stem cell angiogenic capacity and stemness by a biomimetic hydrogel scaffold.* Biomaterials, 2012. **33**(1): p. 80-90.

51. Olivo, C., et al., *In vivo bioluminescence imaging study to monitor ectopic bone formation by luciferase gene marked mesenchymal stem cells.* J Orthop Res, 2008. **26**(7): p. 901-9.

52. Newcomb, J.D., et al., *Timing of cord blood treatment after experimental stroke determines therapeutic efficacy.* Cell Transplant, 2006. **15**(3): p. 213-23.

53. Freyman, T., et al., *A quantitative, randomized study evaluating three methods of mesenchymal stem cell delivery following myocardial infarction.* Eur Heart J, 2006. **27**(9): p. 1114-22.

54. Kim, J., et al., *Proteomic validation of multifunctional molecules in mesenchymal stem cells derived from human bone marrow, umbilical cord blood and peripheral blood.* PLoS One, 2012. **7**(5): p. e32350.

55. Monaco, E., et al., *Transcriptomics comparison between porcine adipose and bone marrow mesenchymal stem cells during in vitro osteogenic and adipogenic differentiation.* PLoS One, 2012. **7**(3): p. e32481.

56. Burdick, J.A., *Injectable gels for tissue/organ repair.* Biomed Mater, 2012. **7**(2): p. 020201.

57. Mountziaris, P.M., et al., *Harnessing and modulating inflammation in strategies for bone regeneration.* Tissue Eng Part B Rev, 2011. **17**(6): p. 393-402.

58. Thomas, M.V. and D.A. Puleo, *Infection, inflammation, and bone regeneration: a paradoxical relationship.* J Dent Res, 2011. **90**(9): p. 1052-61.

59. Mountziaris, P.M. and A.G. Mikos, *Modulation of the inflammatory response for enhanced bone tissue regeneration.* Tissue Eng Part B Rev, 2008. **14**(2): p. 179-86.

60. Blanchard, F., et al., *The dual role of IL-6-type cytokines on bone remodeling and bone tumors.* Cytokine Growth Factor Rev, 2009. **20**(1): p. 19-28.

61. Chambers, T.J., et al., *The role of prostaglandins and nitric oxide in the response of bone to mechanical forces.* Osteoarthritis Cartilage, 1999. **7**(4): p. 422-3.

62. Ankrum, J.A., J.F. Ong, and J.M. Karp, *Mesenchymal stem cells: immune evasive, not immune privileged.* Nat Biotechnol, 2014. **32**(3): p. 252-60.

63. Iyer, S.S. and M. Rojas, *Anti-inflammatory effects of mesenchymal stem cells: novel concept for future therapies.* Expert Opin Biol Ther, 2008. **8**(5): p. 569-81.

64. Zimmermann, J.A. and T.C. McDevitt, *Pre-conditioning mesenchymal stromal cell spheroids for immunomodulatory paracrine factor secretion.* Cytotherapy, 2014. **16**(3): p. 331-45.

65. Bartosh, T.J., et al., *Aggregation of human mesenchymal stromal cells (MSCs) into 3D spheroids enhances their antiinflammatory properties.* Proc Natl Acad Sci U S A, 2010. **107**(31): p. 13724-9.

66. Murphy, K.C., S.Y. Fang, and J.K. Leach, *Human mesenchymal stem cell spheroids in fibrin hydrogels exhibit improved cell survival and potential for bone healing.* Cell Tissue Res, 2014. **357**(1): p. 91-9.

67. Bhang, S.H., et al., *Angiogenesis in ischemic tissue produced by spheroid grafting of human adipose-derived stromal cells.* Biomaterials, 2011. **32**(11): p. 2734-47.

68. Lee, E.J., et al., *Spherical bullet formation via E-cadherin promotes therapeutic potency of mesenchymal stem cells derived from human umbilical cord blood for myocardial infarction.* Mol Ther, 2012. **20**(7): p. 1424-33.

69. Wang, C.C., et al., *Spherically symmetric mesenchymal stromal cell bodies inherent with endogenous extracellular matrices for cellular cardiomyoplasty.* Stem Cells, 2009. **27**(3): p. 724-32.

70. Yamaguchi, Y., et al., *Mesenchymal stem cell spheroids exhibit enhanced in-vitro and in-vivo osteoregenerative potential.* BMC Biotechnol, 2014. **14**(1): p. 105.

71. Wang, W., et al., *3D spheroid culture system on micropatterned substrates for improved differentiation efficiency of multipotent mesenchymal stem cells.* Biomaterials, 2009. **30**(14): p. 2705-15.

72. Shang, F., et al., *The effect of licochalcone A on cell-aggregates ECM secretion and osteogenic differentiation during bone formation in metaphyseal defects in ovariectomized rats.* Biomaterials, 2014. **35**(9): p. 2789-97.

73. Benjamin, S., et al., *Oxygenated environment enhances both stem cell survival and osteogenic differentiation.* Tissue Eng Part A, 2013. **19**(5-6): p. 748-58.

74. Kimelman-Bleich, N., et al., *The use of a synthetic oxygen carrier-enriched hydrogel to enhance mesenchymal stem cell-based bone formation in vivo.* Biomaterials, 2009. **30**(27): p. 4639-48.

75. Tamimi, F., et al., *Perfluorodecalin and bone regeneration.* Eur Cell Mater, 2013. **25**: p. 22-36.

76. Khattak, S.F., et al., *Enhancing oxygen tension and cellular function in alginate cell encapsulation devices through the use of perfluorocarbons.* Biotechnol Bioeng, 2007. **96**(1): p. 156-66.

77. Allen, A.B., et al., *In vivo bioluminescent tracking of mesenchymal stem cells within large hydrogel constructs.* Tissue Eng Part C Methods, 2014. **20**(10): p. 806-16.

78. Sheyn, D., et al., *Gene-modified adult stem cells regenerate vertebral bone defect in a rat model.* Mol Pharm, 2011. **8**(5): p. 1592-601.

79. Sun, N., A. Lee, and J.C. Wu, *Long term non-invasive imaging of embryonic stem cells using reporter genes.* Nat Protoc, 2009. **4**(8): p. 1192-201.

80. Ungrin, M.D., et al., *Reproducible, ultra high-throughput formation of multicellular organization from single cell suspension-derived human embryonic stem cell aggregates.* PLoS One, 2008. **3**(2): p. e1565.

81. Boerckel, J.D., et al., *Effects of protein dose and delivery system on BMP-mediated bone regeneration.* Biomaterials, 2011. **32**(22): p. 5241-51.

82. Noble, B.S. and H.Y. Stevens, *Techniques for the study of apoptosis in bone.* Methods Mol Med, 2003. **80**: p. 225-36.

83. Priddy, L.B., et al., *Oxidized alginate hydrogels for bone morphogenetic protein-2 delivery in long bone defects.* Acta Biomater, 2014.

84. Wiemann, M., et al., *The binding of rhBMP-2 to the receptors of viable MC3T3-E1 cells and the question of cooperativity.* Materialwissenschaft Und Werkstofftechnik, 2001. **32**(12): p. 931-936.

85. Allen, A.B., et al., *In Vivo Bioluminescent Tracking of Mesenchymal Stem Cells Within Large Hydrogel Constructs.* Tissue Eng Part C Methods, 2014.

86. Kolambkar, Y.M., et al., *An alginate-based hybrid system for growth factor delivery in the functional repair of large bone defects.* Biomaterials, 2011. **32**(1): p. 65-74.

87. Oest, M.E., et al., *Quantitative assessment of scaffold and growth factor-mediated repair of critically sized bone defects.* J Orthop Res, 2007. **25**(7): p. 941-50.

88. Thibaudeau, L., et al., *A tissue-engineered humanized xenograft model of human breast cancer metastasis to bone.* Dis Model Mech, 2014. **7**(2): p. 299-309.

89. Kolambkar, Y.M., et al., *Spatiotemporal delivery of bone morphogenetic protein enhances functional repair of segmental bone defects.* Bone, 2011. **49**(3): p. 485-92.

90. Krishnan, L., N.J. Willett, and R.E. Guldberg, *Vascularization strategies for bone regeneration.* Ann Biomed Eng, 2014. **42**(2): p. 432-44.

91. Chim, S.M., et al., *Angiogenic factors in bone local environment.* Cytokine Growth Factor Rev, 2013. **24**(3): p. 297-310.

92. Frith, J.E., B. Thomson, and P.G. Genever, *Dynamic three-dimensional culture methods enhance mesenchymal stem cell properties and increase therapeutic potential.* Tissue Eng Part C Methods, 2010. **16**(4): p. 735-49.

93. Goh, F., et al., *Limited beneficial effects of perfluorocarbon emulsions on encapsulated cells in culture: experimental and modeling studies.* J Biotechnol, 2010. **150**(2): p. 232-9.

94. Sart, S., T. Ma, and Y. Li, *Preconditioning stem cells for in vivo delivery.* Biores Open Access, 2014. **3**(4): p. 137-49.

95. Marie, P.J., *Fibroblast growth factor signaling controlling osteoblast differentiation.* Gene, 2003. **316**: p. 23-32.

96. Fujita, K. and S. Janz, *Attenuation of WNT signaling by DKK-1 and -2 regulates BMP2-induced osteoblast differentiation and expression of OPG, RANKL and M-CSF.* Mol Cancer, 2007. **6**: p. 71.

97. Zhang, C., et al., *Inhibition of Wnt signaling by the osteoblast-specific transcription factor Osterix.* Proc Natl Acad Sci U S A, 2008. **105**(19): p. 6936-41.

98. Kaneshiro, S., et al., *IL-6 negatively regulates osteoblast differentiation through the SHP2/MEK2 and SHP2/Akt2 pathways in vitro.* J Bone Miner Metab, 2014. **32**(4): p. 378-92.

99. Kovach, T.K., et al., *Interactions between MSCs and immune cells: implications for bone healing.* J Immunol Res, 2015. **2015**: p. 752510.

100. Suda, M., et al., *Prostaglandin E2 (PGE2) autoamplifies its production through EP1 subtype of PGE receptor in mouse osteoblastic MC3T3-E1 cells.* Calcif Tissue Int, 1998. **62**(4): p. 327-31.

101. Yokota, K., et al., *Stimulation of prostaglandin E2 synthesis in cloned osteoblastic cells of mouse (MC3T3-E1) by epidermal growth factor.* J Biol Chem, 1986. **261**(33): p. 15410-5.

102. Dey, I., M. Lejeune, and K. Chadee, *Prostaglandin E2 receptor distribution and function in the gastrointestinal tract.* Br J Pharmacol, 2006. **149**(6): p. 611-23.

103. White, J.C., et al., *Addition of perfluorocarbons to alginate hydrogels significantly impacts molecular transport and fracture stress.* J Biomed Mater Res A, 2013. **101**(2): p. 438-46.

FIGURE CAPTIONS

Figure 1 – Effect of hMSC Aggregation on Cell Survival and Construct Composition through 14 Days *In Vivo* A) Prior to subcutaneous implantation, hMSC aggregates (live = GFP (green); dead = ethidium homodimer (red)) were observed to maintain viability and structure following alginate embedding at densities of 0.5 (left) and 2.0 (right) x10^6 cells/150 μL (scale bar = 100 μm). B) *In vitro* BLI counts vs. viable cell number for aggregate-seeded hydrogels displayed a linear correlation (r^2 = 0.75) similar to that of constructs seeded with single hMSCs (r^2 = 0.99). C) Aggregated hMSCs migrated as single cells within the alginate hydrogel over 1 week of culture, as assessed by LDH staining (scale bar = 100 μm). D, E) Following delivery *in vivo*, quantification of normalized BLI signal and representative BLI heatmaps illustrate similarly maintained viability for single hMSCs and aggregates through 14 days post-operatively. F, G) Construct vascular volume at Day 14 was unaffected by hMSC aggregation and vascular reconstructions of representative single cell (left) and aggregate (right) samples colored to indicate vessel diameter demonstrate no qualitative difference in vessel morphology. H) Irrespective of treatment, explants contained alginate pieces surrounded by fibrotic tissue (yellow arrows), as visualized using Masson's trichrome staining. Morphology of alginate-embedded ECM pockets differed between treatments, with single cell delivery resulting in a more qualitatively even distribution (green arrows) while aggregate samples contained multi-node (pink arrows) and branching (red arrows) pockets as well as regions void of ECM pockets (not shown) (scale bar = 100 μm). I) NuMA staining (white arrows) revealed the persistence of delivered single cells within the alginate interior, whereas cells implanted as aggregates were localized to the hydrogel exterior by 14 days (scale bar = 100 μm).

Figure 2 – Effect of hMSC Delivery on Large Bone Defect Repair in Nude Rats A) Longitudinal μCT measurement found no effect of hMSC delivery, either as single cells or aggregates, on regenerate bone volume. However, the lack of co-delivered BMP-2 alongside hMSC aggregates ("Aggregates" group) resulted in a significantly diminished amount of bone tissue (* = $p < 0.05$ vs. BMP-2-containing treatments). B) Maximum torque of the explanted femurs at 12 weeks was highly variable and not significantly affected by method of hMSC delivery (p=0.985) nor BMP-2 treatment (p=0.090). C) Similarly, neither cell group (p=0.942) nor BMP-2 dose (p=0.076) impacted torsional stiffness.

Figure 3 – *In Vitro* Characterization and Hypoxic Culture of rMSC Aggregates A) Similar to hMSCs, rMSCs seeded in agar micro-wells formed aggregates (500 cells/spheroid) over 14 hrs (scale bar = 500 μm). B) rMSCs exhibited increased secretion of the immunomodulatory factors IL-6 and PGE2 over 24 hrs in comparison to rMSCs plated in 2D. C) Intracellular ALP activity normalized to DNA content was also enhanced with rMSC aggregation. D) Single cell (SC) and aggregated (AG) rMSCs were embedded within alginate hydrogels with (+) or without (-) the synthetic oxygen carrier PFTBA. Longitudinal BLI was conducted to monitor cell viability throughout 4 days of culture at hypoxic (3% O_2) conditions. Normalized BLI revealed better-maintained viability for single cell groups and no effect of PFTBA addition (* = $p < 0.05$ as indicated; $ = $p < 0.05$ within treatment vs. Day 2; # = $p < 0.05$ within treatment vs. Days 0 and 2).

Figure 4 – Effect of rMSC Aggregation on Cell Survival and Construct Composition through 14 Days *In Vivo* Acellular (Acell), single cell (SC), and aggregate (AG) treatments with (+) or without (-) PFTBA were delivered to Lewis rats and longitudinally monitored through 14 days using BLI. A, B) As assessed by normalized BLI measurement and representative heatmaps, all groups displayed a decrease in BLI signal through 14 days, indicative of a post-operative drop in viable cell number over time. *In vivo* survival was affected by cell presentation ($p_{SCvs.AG}$=0.009), but not PFTBA incorporation (p_{PFTBA}=0.075). Individual comparisons between treatments and timepoints revealed an increase in viable cell number for the SC- treatment at Day 1 (# = $p < 0.05$ within timepoint vs. all other treatments; $ = $p < 0.05$ within treatment vs. Days 7 and 14). C) Vascular reconstructions illustrate vessel diameter distribution in representative images from each treatment group. Qualitatively, no gross effects of cell delivery group or PFTBA addition were apparent. D) Quantification of construct vascular volume found no overall effect of rMSC or PFTBA delivery. However, single cells constructs without co-delivered PFTBA had significantly more vasculature than acellular, PFTBA-containing constructs. E) All treatment groups contained a similar extent of residual alginate pieces (red asterisks) surrounded by granulation tissue, as visualized through H&E staining (0% PFTBA, cell delivery groups shown; scale bar = 100 μm). F) Fluorescent microscopy revealed the presence and distribution of delivered rMSCs (rMSCs = red (*DiI*); all nuclei = blue (*DAPI*)). Implanted single cells appeared to be retained within alginate pieces and away from regions of high cellularity. rMSCs delivered as spheroids remained clustered, although exhibiting a diameter greater than that of the initially implanted structures (~175 μm vs. ~100 μm), indicating the breakup of rMSC aggregates over time *in vivo*. G) A protocol for HIF-1 alpha immunostaining of HIF-1 alpha subunit translocation to the nuclei of hMSCs was developed using 24-hr application of the hypoxia mimetic desferoxamine (DFO; 50 μM) as a positive control. In the absence of DFO treatment, nuclei appear blue (DAPI counterstain), indicating a lack of HIF-1 alpha translocation. After addition of 50 μM DFO, HIF-1 alpha subunit stabilizes and translocates to the nucleus. Immunolocalization of HIF-1 alpha using rhodamine-conjugated secondary antibody (Dylight 594) in the nucleus causes the nucleus to appear pink/purple (scale bar = 20 μm). H) Confocal microscopy images of delivered rMSCs (red (*DiI*)) immunostained for HIF-1 alpha subunit translocation (green (*hypoxia label 488*)) revealed that hypoxic implanted cells (yellow (*dual-labeled*)) were present within all treatment groups at Day 14 (scale bar = 50 μm).

Figure 5 – Effect of rMSC and PFTBA Delivery on *In Vitro* BMP-2 Release Acellular (Acell), single cell (SC), and aggregated (AG) rMSCs were embedded within alginate/mesh constructs with (+) or without (-) PFTBA and each containing a 1.5-μg dose of BMP-2. Constructs were cultured and conditioned media was collected over 7 days. A) BMP-2 released from the constructs was measured via ELISA. Over the first 24 hrs, all groups released similar amounts of BMP-2. However, following this initial period, acellular constructs released more BMP-2 than constructs seeded with single (p=0.002) or aggregated (p=0.046) rMSCs. There was no effect of PFTBA incorporation during either the first 24 hrs (p=0.143) or remaining (p=0.441) culture period. B) Despite BMP-2 release data, seeding of rMSCs led to increased induction of ALP activity in a pre-osteoblast cell line (MC3T3-E1) exposed to conditioned media. ALP activity was lower for acellular groups conditioned with media from the first 24 hrs in comparison to both rMSC-seeded groups (SC, AG). Media collected from aggregate-containing

constructs at each timepoint induced ALP activity most strongly. Furthermore, PFTBA addition had an early positive effect (p=0.011). Normalized results indicate that changes in ALP activity were not due to altered MC3T3-E1 number alone.

Figure 6 – Effect of rMSC Delivery on Large Bone Defect Repair in Lewis Rats A) Representative mineral density heatmaps generated from 12-week μCT analysis of critically-sized femoral defects treated with acellular (Acell), single cell (SC), and aggregate (AG) containing hydrogels with (+) or without (-) PFTBA showed a qualitative decrease in bone regeneration with rMSC or PFTBA delivery. Consistent with radiograph observations (data not shown), only samples in the Acell- treatment group exhibited bridging of the defect space. B) Quantification of regenerated bone tissue at 12 weeks found that treatment with rMSCs or PFTBA attenuated defect repair in both an individual and additive manner, as measured via *ex vivo* μCT. C) Biomechanical testing revealed that maximum torque was greatest for the Acell-treatment, observing a decrease in tissue mechanics with the addition of rMSCs (p_{SC}=0.001; p_{AG}=0.001) or PFTBA (p=0.018) D) Torsional stiffness values were similar to maximum torque data, with Acell- treatment resulting in the highest value and an observed detrimental effect of rMSC (p_{SC}=0.002; p_{AG}<0.001) or PFTBA (p=0.024) addition. E) Tissue development within the defect space varied with rMSC and PFTBA delivery, as visualized via SafO staining. Injuries treated with acellular hydrogel in the absence of co-delivered PFTBA (Acell-) contained the greatest extent of organized bone (blue) and mineralized alginate (pink) by 12 weeks. In contrast, delivery of rMSCs (singular (SC) or aggregated (AG)) or PFTBA (+) qualitatively decreased the extent of defect mineralization and increased the presence of residual alginate (red). F) Fluorescent microscopy revealed the presence of rMSCs in all cell-treated defects through 12 weeks (rMSCs = red (*DiI*); all nuclei = blue (*DAPI*)). Muted DiI signal, found localized to macrophage-containing regions, was present in a subset of acellular samples as well (rMSC label = red (*DiI*); macrophages = green (*CD68+*)).

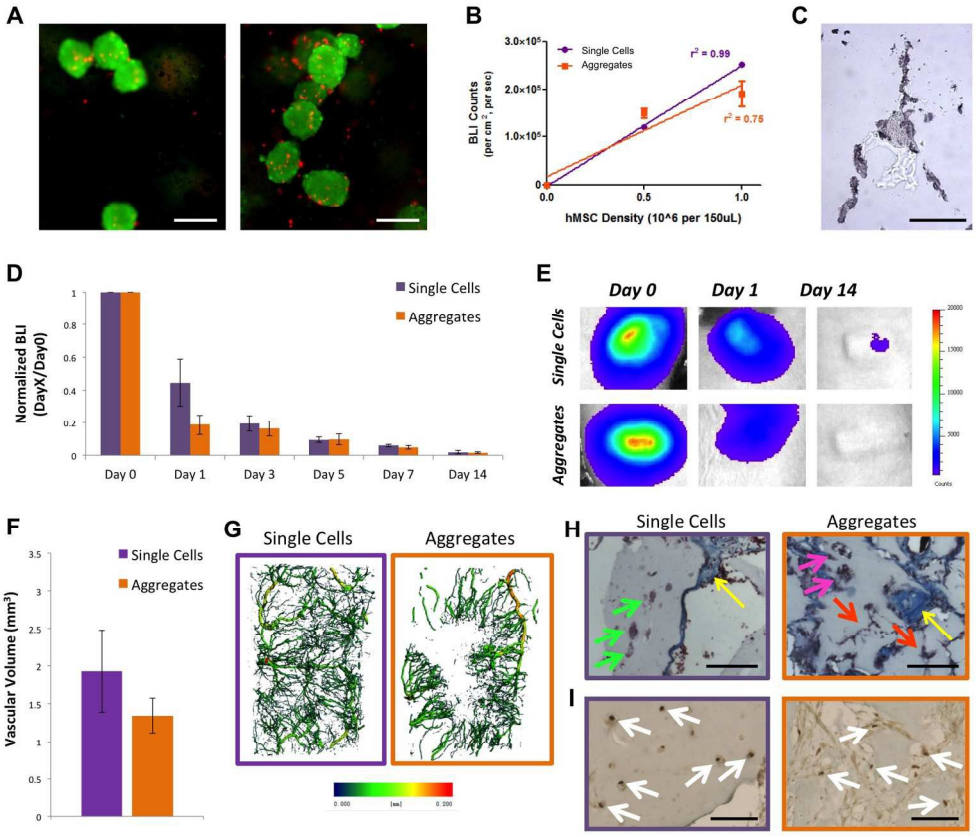

Figure 1 – Effect of hMSC Aggregation on Cell Survival and Construct Composition through 14 Days In Vivo A) Prior to subcutaneous implantation, hMSC aggregates (live = GFP (green); dead = ethidium homodimer (red)) were observed to maintain viability and structure following alginate embedding at densities of 0.5 (left) and 2.0 (right) x106 cells/150 µL (scale bar = 100 µm). B) In vitro BLI counts vs. viable cell number for aggregate-seeded hydrogels displayed a linear correlation (r2 = 0.75) similar to that of constructs seeded with single hMSCs (r2 = 0.99). C) Aggregated hMSCs migrated as single cells within the alginate hydrogel over 1 week of culture, as assessed by LDH staining (scale bar = 100 µm). D, E) Following delivery in vivo, quantification of normalized BLI signal and representative BLI heatmaps illustrate similarly maintained viability for single hMSCs and aggregates through 14 days post-operatively. F, G) Construct vascular volume at Day 14 was unaffected by hMSC aggregation and vascular reconstructions of representative single cell (left) and aggregate (right) samples colored to indicate vessel diameter demonstrate no qualitative difference in vessel morphology. H) Irrespective of treatment, explants contained alginate pieces surrounded by fibrotic tissue (yellow arrows), as visualized using Masson's trichrome staining. Morphology of alginate-embedded ECM pockets differed between treatments, with single cell delivery resulting in a more qualitatively even distribution (green arrows) while aggregate samples contained multi-node (pink arrows) and branching (red arrows) pockets as well as regions void of ECM pockets (not shown) (scale bar = 100 µm). I) NuMA staining (white arrows) revealed the persistence of delivered single cells within the alginate interior, whereas cells implanted as aggregates were localized to the hydrogel exterior by 14 days (scale bar = 100 µm).
705x604mm (72 x 72 DPI)

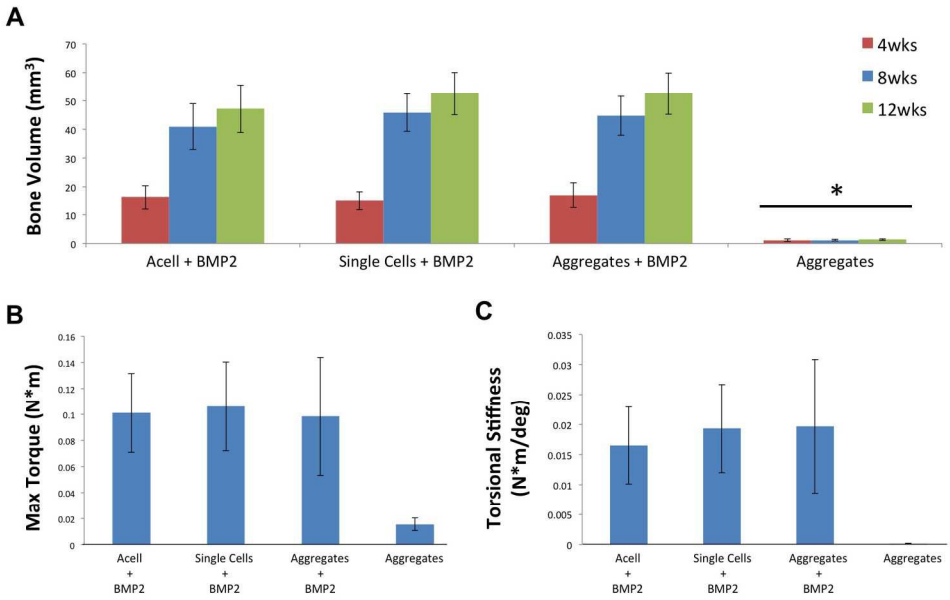

Figure 2 – Effect of hMSC Delivery on Large Bone Defect Repair in Nude Rats A) Longitudinal μCT measurement found no effect of hMSC delivery, either as single cells or aggregates, on regenerate bone volume. However, the lack of co-delivered BMP-2 alongside hMSC aggregates ("Aggregates" group) resulted in a significantly diminished amount of bone tissue (* = $p < 0.05$ vs. BMP-2-containing treatments). B) Maximum torque of the explanted femurs at 12 weeks was highly variable and not significantly affected by method of hMSC delivery ($p=0.985$) nor BMP-2 treatment ($p=0.090$). C) Similarly, neither cell group ($p=0.942$) nor BMP-2 dose ($p=0.076$) impacted torsional stiffness.
705x434mm (72 x 72 DPI)

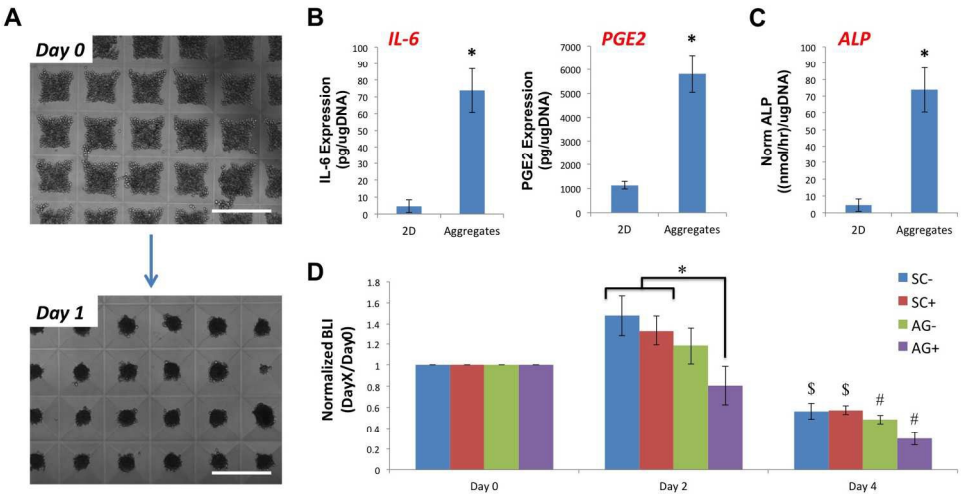

Figure 3 – In Vitro Characterization and Hypoxic Culture of rMSC Aggregates A) Similar to hMSCs, rMSCs seeded in agar micro-wells formed aggregates (500 cells/spheroid) over 14 hrs (scale bar = 500 μm). B) rMSCs exhibited increased secretion of the immunomodulatory factors IL-6 and PGE2 over 24 hrs in comparison to rMSCs plated in 2D. C) Intracellular ALP activity normalized to DNA content was also enhanced with rMSC aggregation. D) Single cell (SC) and aggregated (AG) rMSCs were embedded within alginate hydrogels with (+) or without (-) the synthetic oxygen carrier PFTBA. Longitudinal BLI was conducted to monitor cell viability throughout 4 days of culture at hypoxic (3% O2) conditions. Normalized BLI revealed better-maintained viability for single cell groups and no effect of PFTBA addition (* = $p < 0.05$ as indicated; $ = $p < 0.05$ within treatment vs. Day 2; # = $p < 0.05$ within treatment vs. Days 0 and 2).
705x391mm (72 x 72 DPI)

FIGURE 4

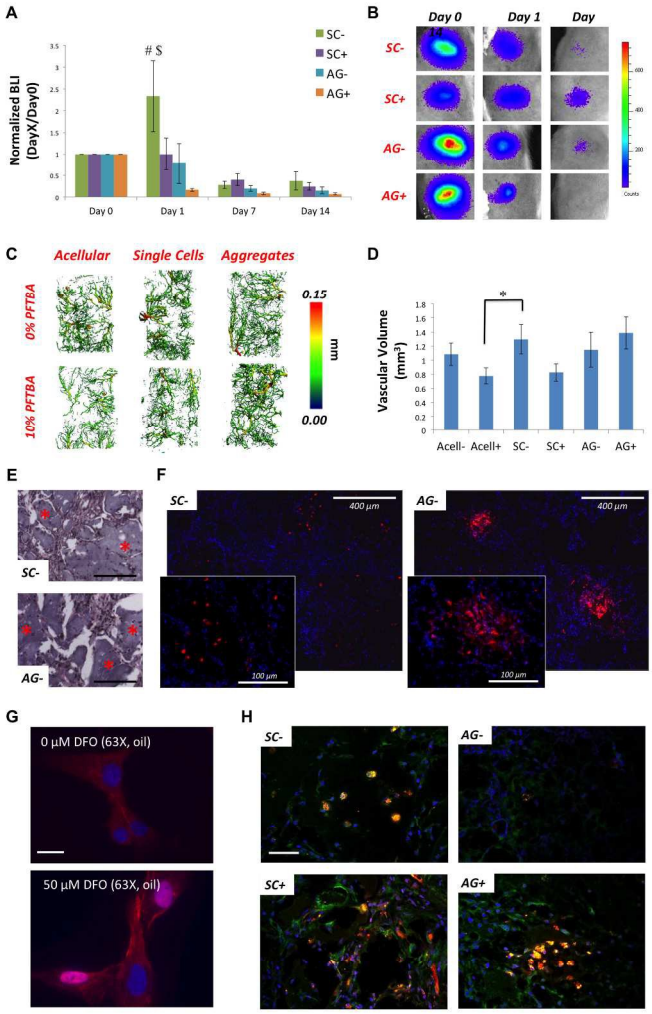

Figure 4 – Effect of rMSC Aggregation on Cell Survival and Construct Composition through 14 Days In Vivo Acellular (Acell), single cell (SC), and aggregate (AG) treatments with (+) or without (-) PFTBA were delivered to Lewis rats and longitudinally monitored through 14 days using BLI. A, B) As assessed by normalized BLI measurement and representative heatmaps, all groups displayed a decrease in BLI signal through 14 days, indicative of a post-operative drop in viable cell number over time. In vivo survival was affected by cell presentation (pSCvs.AG=0.009), but not PFTBA incorporation (pPFTBA=0.075). Individual comparisons between treatments and timepoints revealed an increase in viable cell number for the SC- treatment at Day 1 (# = $p < 0.05$ within timepoint vs. all other treatments; $ = $p < 0.05$ within treatment vs. Days 7 and 14). C) Vascular reconstructions illustrate vessel diameter distribution in representative images from each treatment group. Qualitatively, no gross effects of cell delivery group or PFTBA addition were apparent. D) Quantification of construct vascular volume found no overall effect of rMSC or PFTBA delivery. However, single cells constructs without co-delivered PFTBA had significantly more vasculature than acellular, PFTBA-containing constructs. E) All treatment groups contained a similar extent of residual

alginate pieces (red asterisks) surrounded by granulation tissue, as visualized through H&E staining (0% PFTBA, cell delivery groups shown; scale bar = 100 μm). F) Fluorescent microscopy revealed the presence and distribution of delivered rMSCs (rMSCs = red (DiI); all nuclei = blue (DAPI)). Implanted single cells appeared to be retained within alginate pieces and away from regions of high cellularity. rMSCs delivered as spheroids remained clustered, although exhibiting a diameter greater than that of the initially implanted structures (~175 μm vs. ~100 μm), indicating the breakup of rMSC aggregates over time in vivo. G) A protocol for HIF-1 alpha immunostaining of HIF-1 alpha subunit translocation to the nuclei of hMSCs was developed using 24-hr application of the hypoxia mimetic desferoxamine (DFO; 50 μM) as a positive control. In the absence of DFO treatment, nuclei appear blue (DAPI counterstain), indicating a lack of HIF-1 alpha translocation. After addition of 50 μM DFO, HIF-1 alpha subunit stabilizes and translocates to the nucleus. Immunolocalization of HIF-1 alpha using rhodamine-conjugated secondary antibody (Dylight 594) in the nucleus causes the nucleus to appear pink/purple (scale bar = 20 μm). H) Confocal microscopy images of delivered rMSCs (red (DiI)) immunostained for HIF-1 alpha subunit translocation (green (hypoxia label 488)) revealed that hypoxic implanted cells (yellow (dual-labeled)) were present within all treatment groups at Day 14 (scale bar = 50 μm).
705x1058mm (72 x 72 DPI)

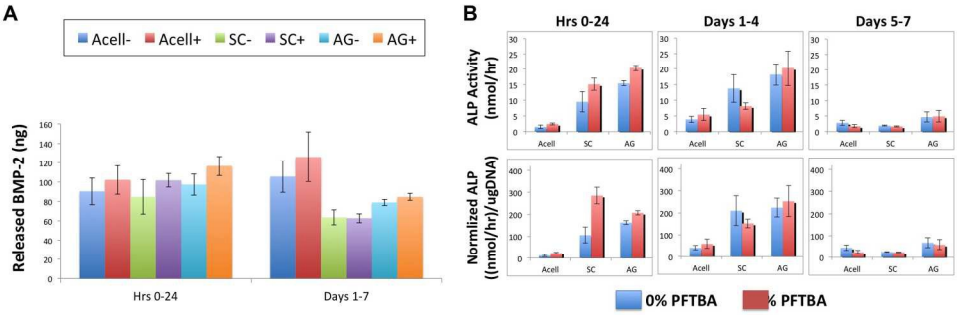

Figure 5 – Effect of rMSC and PFTBA Delivery on In Vitro BMP-2 Release Acellular (Acell), single cell (SC), and aggregated (AG) rMSCs were embedded within alginate/mesh constructs with (+) or without (-) PFTBA and each containing a 1.5-μg dose of BMP-2. Constructs were cultured and conditioned media was collected over 7 days. A) BMP-2 released from the constructs was measured via ELISA. Over the first 24 hrs, all groups released similar amounts of BMP-2. However, following this initial period, acellular constructs released more BMP-2 than constructs seeded with single ($p=0.002$) or aggregated ($p=0.046$) rMSCs. There was no effect of PFTBA incorporation during either the first 24 hrs ($p=0.143$) or remaining ($p=0.441$) culture period. B) Despite BMP-2 release data, seeding of rMSCs led to increased induction of ALP activity in a pre-osteoblast cell line (MC3T3-E1) exposed to conditioned media. ALP activity was lower for acellular groups conditioned with media from the first 24 hrs in comparison to both rMSC-seeded groups (SC, AG). Media collected from aggregate-containing constructs at each timepoint induced ALP activity most strongly. Furthermore, PFTBA addition had an early positive effect ($p=0.011$). Normalized results indicate that changes in ALP activity were not due to altered MC3T3-E1 number alone.
705x264mm (72 x 72 DPI)

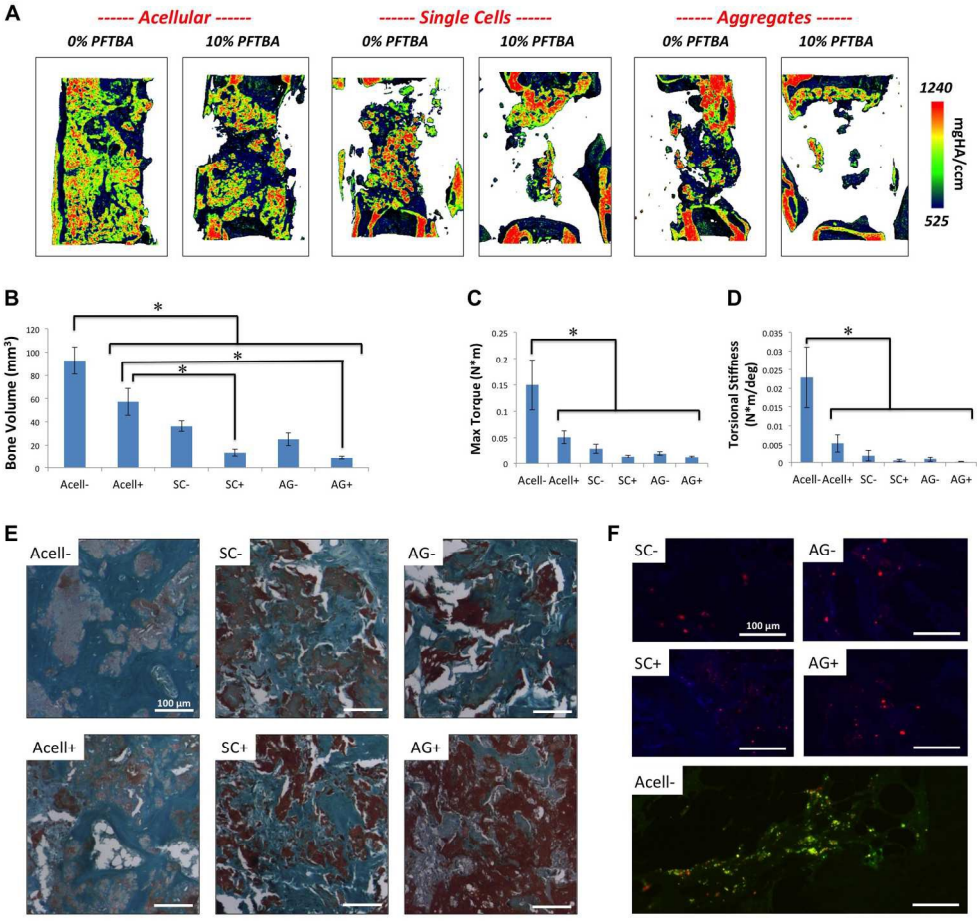

Figure 6 – Effect of rMSC Delivery on Large Bone Defect Repair in Lewis Rats A) Representative mineral density heatmaps generated from 12-week µCT analysis of critically-sized femoral defects treated with acellular (Acell), single cell (SC), and aggregate (AG) containing hydrogels with (+) or without (-) PFTBA showed a qualitative decrease in bone regeneration with rMSC or PFTBA delivery. Consistent with radiograph observations (data not shown), only samples in the Acell- treatment group exhibited bridging of the defect space. B) Quantification of regenerated bone tissue at 12 weeks found that treatment with rMSCs or PFTBA attenuated defect repair in both an individual and additive manner, as measured via ex vivo µCT. C) Biomechanical testing revealed that maximum torque was greatest for the Acell- treatment, observing a decrease in tissue mechanics with the addition of rMSCs (pSC=0.001; pAG=0.001) or PFTBA (p=0.018) D) Torsional stiffness values were similar to maximum torque data, with Acell- treatment resulting in the highest value and an observed detrimental effect of rMSC (pSC=0.002; pAG<0.001) or PFTBA (p=0.024) addition. E) Tissue development within the defect space varied with rMSC and PFTBA delivery, as visualized via SafO staining. Injuries treated with acellular hydrogel in the absence of co-delivered PFTBA (Acell-) contained the greatest extent of organized bone (blue) and mineralized alginate (pink) by 12 weeks. In contrast, delivery of rMSCs (singular (SC) or aggregated (AG)) or PFTBA (+) qualitatively decreased the extent of defect mineralization and increased the presence of residual alginate (red). F) Fluorescent microscopy revealed the presence of rMSCs in all cell-treated defects through 12 weeks (rMSCs = red (DiI); all nuclei = blue (DAPI)). Muted DiI signal, found localized to macrophage-containing regions, was present in a subset of acellular samples as well (rMSC label = red (DiI); macrophages = green (CD68+)).
705x682mm (72 x 72 DPI)

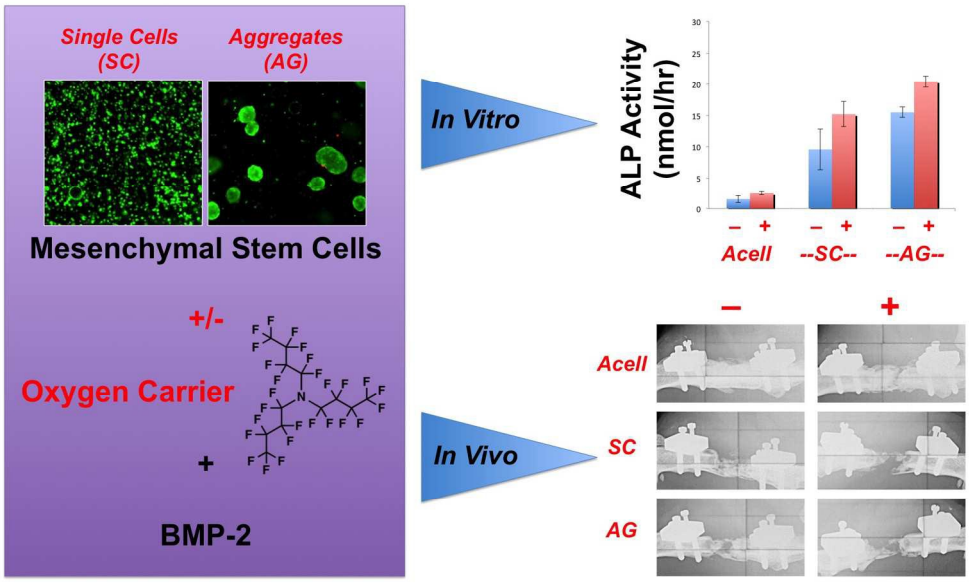

705x440mm (72 x 72 DPI)